An Oxford SWIFT Integral Field Spectroscopy study of 14 early-type galaxies in the Coma cluster

Nicholas Scott,[1,2][*] Ryan Houghton,[2] Roger L. Davies,[2] Michele Cappellari,[2] Niranjan Thatte,[2] Fraser Clarke,[2] Matthias Tecza[2]

[1]*Centre for Astrophysics & Supercomputing, Swinburne University of Technology, PO Box 218, Hawthorn, VIC 3122, Australia*
[2]*Sub-Dept. of Astrophysics, Dept. of Physics, University of Oxford, Denys Wilkinson Building, Keble Road, Oxford, OX1 3RH, UK*

May 2012

ABSTRACT

As a demonstration of the capabilities of the new Oxford SWIFT integral field spectrograph, we present first observations for a set of 14 early-type galaxies in the core of the Coma cluster. Our data consist of *I*- and *z*-band spatially resolved spectroscopy obtained with the Oxford SWIFT spectrograph, combined with *r*-band photometry from the SDSS archive for 14 early-type galaxies. We derive spatially resolved kinematics for all objects from observations of the calcium triplet absorption features at ~ 8500 Å. Using this kinematic information we classify galaxies as either Fast Rotators or Slow Rotators. We compare the fraction of fast and slow rotators in our sample, representing the densest environment in the nearby Universe, to results from the ATLAS[3D] survey, finding the slow rotator fraction is ~ 50 per cent larger in the core of the Coma cluster than in the volume-limited ATLAS[3D] sample, a 1.2 σ increase given our selection criteria. Comparing our sample to the Virgo cluster core only (which is 24 times less dense than the Coma core) we find no evidence of an increase in the slow rotator fraction. Combining measurements of the effective velocity dispersion σ_e with the photometric data we determine the Fundamental Plane for our sample of galaxies. We find the use of the average velocity dispersion within 1 effective radius, σ_e, reduces the residuals by 13 per cent with respect to comparable studies using central velocity dispersions, consistent with other recent integral field Fundamental Plane determinations.

Key words: galaxies: elliptical and lenticular, cD - galaxies: clusters: individual: Coma cluster - galaxies: kinematics and dynamics.

1 INTRODUCTION

In the local Universe, integral field spectroscopy surveys have shed new light on the formation and evolution of nearby early-type galaxies (ETGs). In particular, two dimensional information has led to a significant revision of the way we classify these objects. ETGs had long been known to exhibit a range of kinematic types, from the traditional picture of giant, pressure-supported elliptical galaxies (Binney 1982) to less massive, rotationally supported systems (Davies et al. 1983). The SAURON (de Zeeuw et al. 2002) and ATLAS[3D] (Cappellari et al. 2011a) surveys improved this classification system to take advantage of integral field spectroscopy, basing their classification on the observed specific stellar angular momentum of a galaxy, λ_R (Emsellem et al. 2007). Emsellem et al. (2011) classified galaxies into fast-rotators (FRs, $\lambda_R/\sqrt{\epsilon} > 0.31$) and slow-rotators (SRs, $\lambda_R/\sqrt{\epsilon} \leqslant 0.31$, where ϵ is the galaxy's ellipticity). This classification system differs significantly from the traditional E/S0 morphological classification, with the majority of early-types being FRs and only a small fraction being SRs (14 per cent in the ATLAS[3D] survey, compared to 27 per cent being classified 'elliptical'). This classification scheme provides an interesting new perspective on the morphology-density relation (Dressler 1980). Dividing galaxies into spirals, FRs and SRs, Cappellari et al. (2011b) find that the fraction of all galaxies that are FRs increases linearly with environment, in the sense that the densest environments have a higher proportion of FRs. In contrast they find that the fraction of all galaxies that are SRs (and correspondingly the fraction of ETGs that are SRs) increases only in the densest environment covered by the ATLAS[3D] survey, the core of the Virgo cluster. By determining the fraction of ETGs that are SRs (N_{SR}/N_{ETG}, hereafter the SR fraction) in the Coma cluster, the densest environment in the nearby Universe, we can extend the kinematic morphology-density relation to denser environments and gain insight into which physical processes give rise to this relation.

Perhaps the key tool in understanding and interpreting ETG structure is the Fundamental Plane (FP): the observed relationship between the effective radius, R_e, effective surface brightness, $\langle\mu\rangle_e$

Table 1. Photometric and spectroscopic parameters of the SWIFT IFS Coma ETG sample

Name	Exposure Time (s)	R_e (arcsec)	$\langle \mu_{e,r} \rangle$ (mag arcsec^{-2})	ϵ	σ_e (km s^{-1})	Fractional IFS Coverage	λ_R	Classification
(1)	(2)	(3)	(4)	(5)	(6)	(7)	(8)	(9)
PGC44679	3600	4.07	18.81	0.14	119 ± 6	1.0	0.11	SR
IC4011	3600	5.41	19.12	0.07	105 ± 8	0.58	0.28	FR
IC4051	2400	17.67	19.93	0.19	231 ± 16	0.46	0.04	SR
NGC4860	1800	6.99	18.27	0.15	213 ± 9	1.0	0.10	SR
NGC4867	2400	2.35	16.98	0.30	183 ± 10	1.0	0.20	FR
NGC4872	1800	4.35	18.05	0.23	213 ± 14	1.0	0.34	FR
NGC4873	3600	8.57	19.24	0.21	153 ± 11	1.0	0.17	FR
NGC4874	4800	54.31	20.78	0.07	200 ± 26	0.31	0.08	SR
NGC4883	2700	7.49	18.99	0.17	149 ± 11	1.0	0.15	FR
NGC4886	3600	7.16	18.93	0.03	128 ± 11	1.0	0.06	FR
NGC4889	1800	31.61	19.45	0.30	375 ± 32	0.56	0.11	SR
PGC44533	3600	4.95	19.66	0.23	94 ± 5	0.92	0.20	FR
PGC44602*	3600	6.00	19.78	0.36	79 ± 5	0.75	0.21	FR
PGC44662	2400	4.46	18.68	0.28	127 ± 5	0.99	0.22	FR

* Observed with the 0.16 arcsec pixel scale

Columns: (1) Galaxy name from Hyperleda. (3) Effective radius, typical error 10 per cent. (4) Average surface brightness within one R_e, typical error 10 per cent. (5) Ellipticity measured at 1 R_e. (6) Effective velocity dispersion. (7) Fraction of 1 R_e covered by the SWIFT IFS field-of-view. (8) λ parameter measured at 1 R_e. Typical errors on λ_R are ~ 5 per cent. (9) Kinematic classification as Emsellem et al. (2011): SR = Slow Rotator, FR = Fast Rotator.

and velocity dispersion (σ) of a galaxy. The tight observed relationship between these quantities, first noted by Djorgovski & Davis (1987) and Dressler et al. (1987), has been used to interpret the structure and evolution of ETGs. This is possible because the Virial Theorem predicts a FP relationship for relaxed, dynamically hot stellar systems (see e.g. Binney & Merrifield 1998). The observed FP is found to be tilted relative to the Virial Theorem prediction, as well as showing small but non-zero intrinsic scatter. The tilt and intrinsic scatter of the observed FP contain significant information about the structure of ETGs (see Renzini & Ciotti 1993, for a summary of some possible physical origins of the FP tilt). An IFS study of ETGs in a single cluster brings two key improvements to the currently available FP observations: i) by selecting only cluster members we select galaxies at a single common distance, eliminating errors in distance as a source of observed scatter in the FP and ii) most studies of the FP have relied upon measurements of the central velocity dispersion σ_c, whereas the Virial Theorem prediction for the FP relates to global variables; specifically, σ_{global} which is better represented by σ_e, which can only be measured using integral field spectroscopy.

In a future work we will present dynamical models of all galaxies in our sample (for which IFS data is a key ingredient), allowing us to construct the mass plane (relating galaxy mass to σ_e and R_e – Bolton et al. 2007) for ETGs in the Coma cluster. We will also use stellar population modelling to derive metallicities from the calcium triplet and use these to explore correlations between the stellar populations, dynamics and metallicity gradients of the galaxies in our sample.

In Section 2 we present our Coma ETG sample including details of how it was selected and outline the observations. In Section 3 we discuss the measurement of the photometric properties of our sample galaxies, the reduction of the SWIFT IFS data and the measurement of the kinematic properties. We then compare the results of our analysis to that of the ATLAS^{3D} survey in Section 4. In Section 5 we briefly present the Fundamental Plane for the initial SWIFT IFS Coma sample.

2 SAMPLE AND OBSERVATIONS
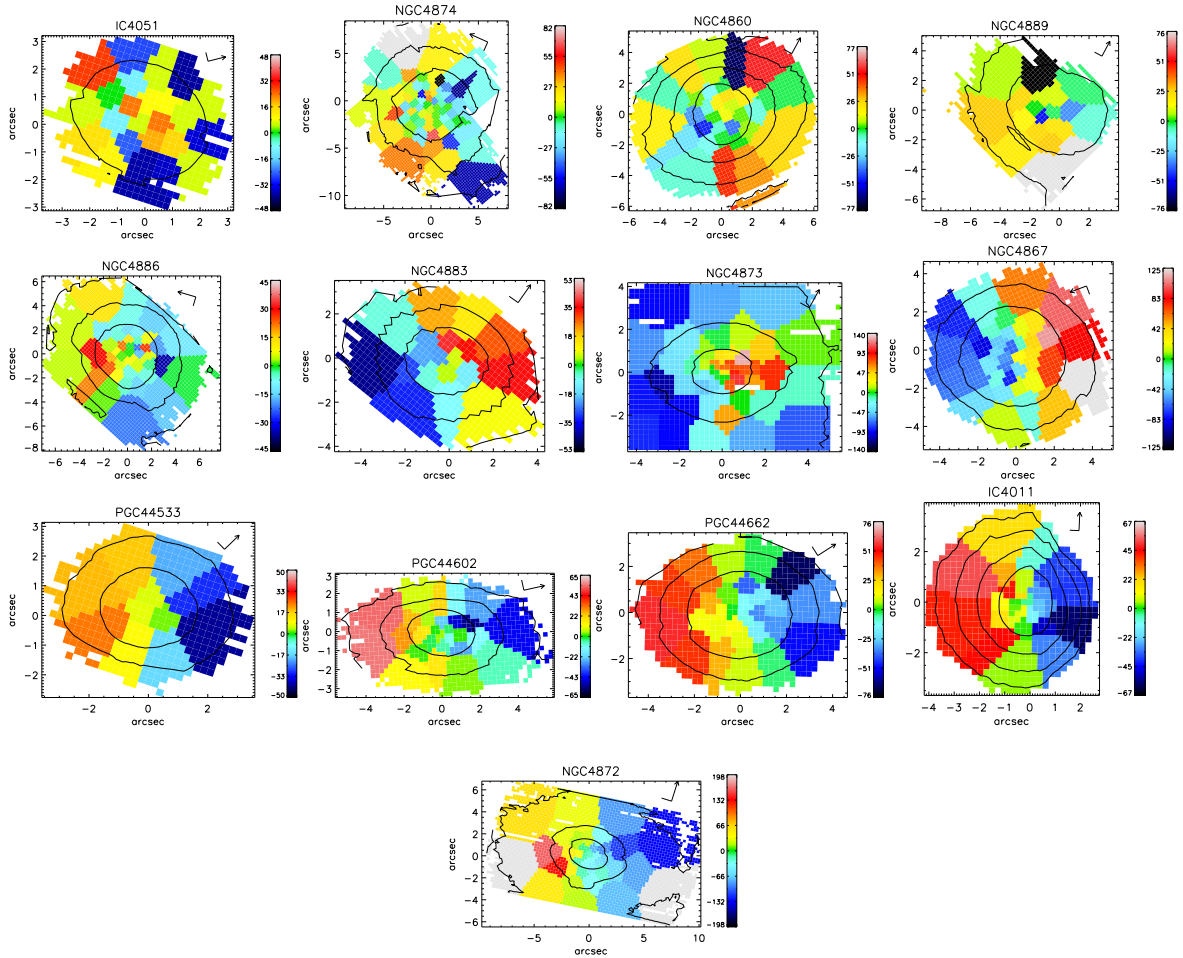
2.1 Sample

The sample of this SWIFT IFS Coma study consists of 14 ETGs, selected from the catalogue of Scodeggio et al. (1998). Our galaxies lie within 0.25 degrees (~ 0.2 Mpc) of the centre of the Coma cluster (RA = $12^h 59^m 36^s$, DEC = $+27° 58'$ Hammer et al. 2010). Sparke & Gallagher (2007) define the region within 0.2 Mpc of the cluster centre as the core region and in their table 7.1 give a density for this region of 13,429 galaxies Mpc^{-3}, the densest region in the local Universe. We divided the Scodeggio et al. (1998) catalogue into seven logarithmically spaced bins in velocity dispersion. From each bin we selected two galaxies, giving reasonable sampling of the range of velocity dispersions and masses found in ETGs in the Coma cluster. Properties of the current SWIFT IFS sample are given in Table 1.

2.2 IFS Observations

Our IFS observations were carried out using the Short Wavelength Integral Field specTrograph (SWIFT, Thatte et al. 2006), an integral field spectrograph based on the image slicer concept with wavelength coverage from 6500 to 10500 Å. The SWIFT IFS is mounted on the Cassegrain focus of the 200" Hale Telescope at the Palomar Observatory in California. The observations were carried out over three separate observing runs (3rd/4th of May 2009, 25th/26th March 2010, 5th June 2010), using the largest 0.235 arcsec pixel^{-1} spatial scale with a field-of-view of 10.3 x 20.9 arcsec^2. For the three largest galaxies (IC4051, NGC4874 and NGC4889) we mosaiced multiple pointings to increase the IFS coverage towards 1 R_e. The seeing varyied between 0.9 and 2 arcseconds, with a median value of 1.3 arcseconds.

2.3 Imaging

Optical *r*-band images for the full sample were obtained from the Sloan Digital Sky Survey (SDSS, York et al. 2000) Data Release 7

Figure 1. Velocity maps for 13 Coma ETGs in the SWIFT IFS sample. The top row shows the 4 SRs, the remaining rows show the FRs. The range of velocities in each map is given by the adjacent colour bar. Representative isophotes from the SWIFT data are overplotted. The maps are rotated such that the photometric position angle is aligned with the x axis. The N–E direction is indicated with the arrow and dash in the upper right corner of each panel.

(Abazajian et al. 2009), via the Montage (Berriman et al. 2004) web service[1], which automatically mosaics, flux calibrates and background subtracts individual SDSS fields. The final images have a spatial scale of 0.4 arcsec pixel^{-1} and were obtained in median seeing of 1.4 arcseconds.

3 DATA ANALYSIS

3.1 Photometric quantities

Photometric quantities (ϵ, R_e and $\langle\mu_{e,r}\rangle$) were measured from the SDSS r-band images. We made used the curve of growth technique (e.g. Cappellari et al. 2006) to determine R_e and $\langle\mu_{e,r}\rangle$ directly from the sky-subtracted images. We determined the ellipticity from the moment technique described in Cappellari et al. (2007). Using the IDL routine *find_galaxy*[2], the second moments of the luminosity distribution were determined for all pixels belonging to the galaxy above a fixed brightness, the level being chosen such that the pixels selected encompass a region with radius 1 R_e or matching the extent of the IFS observations, whichever is the smaller. The ellipticity

was then derived from the observed second moments of the luminosity distribution, which is directly comparable to the measurements presented in the ATLAS^{3D} survey (Emsellem et al. 2011). The photometric quantities are given in Table 1.

3.2 Spectroscopic quantities

3.2.1 Data Reduction

The SWIFT IFS data were reduced using a dedicated IRAF-based pipeline, *swiftred* (Houghton et al., in preparation). The pipeline involves the standard data reduction steps of bias subtraction, flat-fielding, illumination correction, image reconstruction and wavelength calibration. In addition, cosmic rays were removed using the LACOSMIC routine of van Dokkum (2001), implemented in the *swiftred* package. We make use of the OH night sky emission lines (using the emission line atlas of Hanuschik 2003) in the science observations to provide an additional wavelength calibration and spatial flexure correction data. The final wavelength calibration is accurate to ~ 0.1 Å. The sky spectrum was removed by subtracting blank sky frames adjacent in time to each science exposure. The subtraction of sky emission lines was accurate to ~ 2 per cent of the emission line flux.

---

[1] *http://hachi.ipac.caltech.edu:8080/montage*
[2] Available as part of the MGE package of Cappellari (2002).

3.2.2 Kinematics

We extract the stellar kinematics using the penalised PiXel Fitting (pPXF)[3] technique of Cappellari & Emsellem (2004). pPXF uses a library of stellar spectra to produce a template spectrum and convolves this with a line of sight velocity distribution (LOSVD) to best match the observations. We constrain the LOSVD to have a Gaussian shape – we do not fit for the higher-order Gauss-Hermite moments. For fitting the CaT absorption features we used the stellar spectra library of Cenarro et al. (2001), which contains ~ 700 spectra of stars covering a broad range in age and metallicity. Any residuals from cosmic rays or inaccurate sky subtraction were cleaned at this stage by rejecting data points with residuals $> 3\sigma$ from the model spectrum (using the keyword /CLEAN in the pPXF software) and repeating the fit. Only a single rejection iteration was required to produce stable measurements. Large sky residuals were masked from the fitting process.

For galaxies where the IFS field of view was $> 2\ R_e$, an R_e aperture spectrum was formed by binning all pixels lying within an elliptical aperture with area πR_e^2 and ellipticity ϵ_e. For galaxies larger than this an aperture spectrum was formed by accreting spaxels into an aperture of ellipticity ϵ_e until the S/N dropped below 2 per spectral pixel. At this point the diminishing returns from adding additional pixels makes little difference to the quality of the aperture spectrum or the accuracy of the measured σ_e. The fraction of R_e covered by this aperture spectrum is given in Column 7 of Table 1. We measure the mean recession velocity V and effective velocity dispersion σ_e from these aperture spectra (Table 1). For those galaxies where our integrated aperture does not extend to $1R_e$ we correct the measured dispersion according to Eqn. (1) from Cappellari et al. (2006). The magnitude of this correction is small – for NGC4874 (the galaxy with the smallest fractional coverage of R_e) it is only 8 per cent.

To measure λ_R for our galaxies we require spatially resolved kinematics. As the object flux (hence the S/N) decreases rapidly with radius it was necessary to spatially bin the data to determine reliable kinematics at large radii. We made use of the Voronoi binning technique of Cappellari & Copin (2003) to achieve this. A S/N threshold of 40 was selected as the best compromise between extracting robust kinematics from each bin and giving good spatial coverage of each galaxy. Spaxels with a S/N < 2 were excluded from the Voronoi binning. pPXF was again used to determine V and σ for each bin, using the template spectrum determined from the previous fit to the R_e aperture spectrum. This procedure generated V and σ maps for each galaxy in our sample; the V maps are shown in Figure 1.

4 ENVIRONMENTAL DEPENDENCE OF SLOW AND FAST ROTATORS

From the V and σ maps described in the previous section we determine λ_R for each of the galaxies in our sample using Eq. 6 of Emsellem et al. (2007). In Figure 2 we show the distribution of our galaxies in the $\lambda_R - \epsilon$ plane. The solid black line marks the divide between SRs and FRs. The result of our measurements of λ_R and the corresponding FR/SR classification is given in Table 1. For PGC044679 the data quality was too poor to reliably determine λ_R. Excluding PGC044679, we find 4 SRs and 9 FRs in the SWIFT IFS Coma ETG sample. This gives a SR fraction of 4/13 or 31 ± 15 per

[3] Available from http://purl.org/cappellari/idl
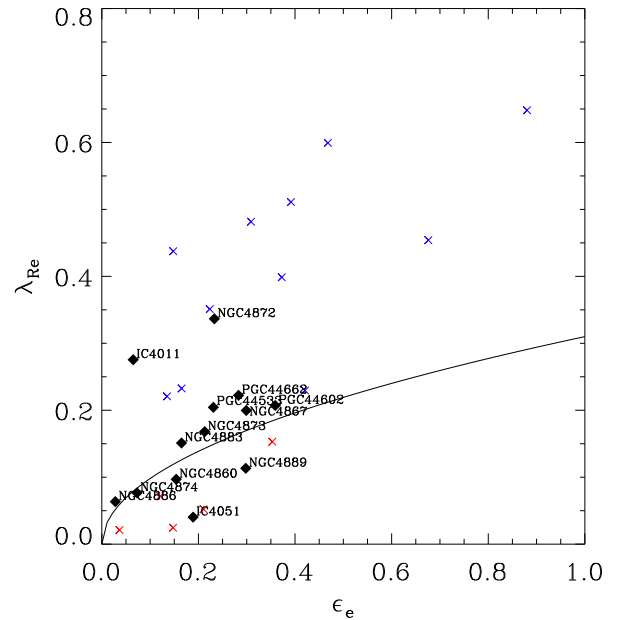
Figure 2. The λ_{R_e} - ϵ diagram for the SWIFT IFS Coma ETG sample. The solid black line shows the divide between SRs and FRs given by $0.31\sqrt{\epsilon}$. 4/13 galaxies in our sample are SRs. We exclude PGC044679 from our analysis due to poor quality IFS data. The red and blue crosses indicate the position SRs and FRs respectively from the core of the Virgo cluster from Emsellem et al. (2011).

cent. NGC4886, despite having a low value of λ_{R_e}, is extremely round ($\epsilon = 0.03$) and so likely to be very close to face on.

The Coma cluster is the densest environment in the local Universe, hence is an ideal place to search for environmental effects on galaxy properties. We make use of the ATLAS[3D] survey (Cappellari et al. 2011a) to provide comparison data in lower density environments. We divide the ATLAS[3D] sample into Virgo and non-Virgo galaxies, representing intermediate and low density environments respectively. The dependence of kinematic type on local environment for the ATLAS[3D] sample is presented in Cappellari et al. (2011b). The principal drawback of our Coma ETG sample is that it is not volume limited - we only observe a fraction of the total ETG population of the Coma cluster. Fortunately the ATLAS[3D] survey is a volume-limited survey, which allows us to ask the question: "If we apply our sample selection criteria to the ATLAS[3D] sample, what is the probability that we reproduce the SR fraction and distribution we find for our Coma sample?"

Using σ_e for the ATLAS[3D] sample obtained from the SAURON data (Cappellari, private communication) we use a Monte Carlo technique to extract samples of galaxies according to our Coma sample selection criteria from both the Virgo and non-Virgo ATLAS[3D] samples. For each mock sample we determine the SR fraction to estimate the likelihood of 'observing' a particular SR fraction given the actual SR fraction, the σ distribution and our sample selection criteria.

In Figure 3 we plot the Monte Carlo expectation of the SR fraction (given our sample selection criteria) for each environment against the projected local environmental density. Densities for the Virgo and non-Virgo ATLAS[3D] samples are taken from Cappellari et al. (2011b) and the density of the Coma cluster core is determined as described in the following paragraph. We use the ρ_{10} density estimator, defined as the number density of galaxies in a sphere enclosing the ten nearest neighbour objects. We find lit-
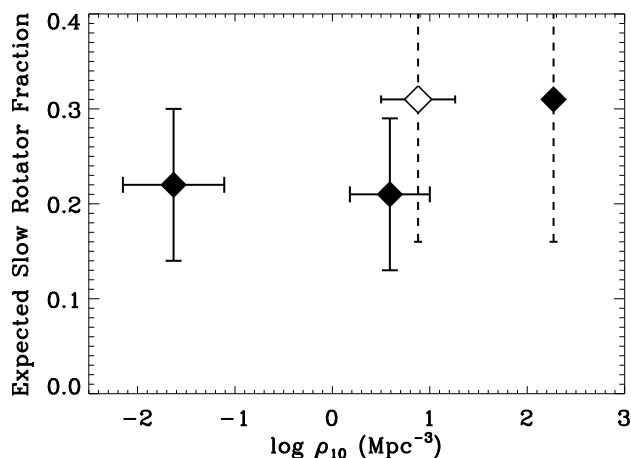
Figure 3. The dependence of the slow rotator fraction on the local environment. The first two solid points show the Monte Carlo expectation from the non-Virgo and Virgo ATLAS^{3D} subsamples, given the SWIFT IFS Coma sample selection. The third solid point is from the SWIFT IFS Coma ETG sample. For the Coma datapoint no error is shown on environmental density due to the more limited sample size and selection. The error on the SR fraction is a Poisson error only and is not appropriate to compare to the ATLAS^{3D} data points. The open data point shows the *observed* (not matched to our sample selection criteria) slow rotator fraction in the core of the Virgo cluster from the ATLAS^{3D} survey. Note the marginal increase in the slow rotator fraction in both cluster cores compared to lower density environments but the lack of an increase in the much denser Coma core compared to the Virgo core.

tle difference in the Monte Carlo expectation of the SR fraction for the ATLAS^{3D} Virgo and field samples. This is consistent with Cappellari et al. (2011b) who, for their complete, volume-limited samples, found that the mean SR fraction in Virgo is only 16 per cent, similar to the field. Our SR fraction of 31 ± 15 per cent represents an increase of 1.2 σ over the ATLAS^{3D} Virgo and field subsamples.

Because our sample is drawn from the core of the Coma cluster we also compare our SR fraction to that found in the core of the Virgo cluster by the ATLAS^{3D} survey. Sparke & Gallagher (2007) define the core of the Virgo cluster to be the region within 0.4 Mpc of the cluster centre (RA = $12^{h}28^{m}19^{s}$, DEC = $+12°40'$ Mould et al. 2000). In their table 7.1 they give the density of this region as 559 galaxies Mpc^{-3}, 24 times less than that in the core of the Coma cluster. The ATLAS^{3D} core Virgo region consists of 16 galaxies – too small a sample to match to our Coma selection criteria using the method described above – so we compare the observed slow rotator fractions only. Cappellari et al. (2011b) find 5/16 galaxies in the Virgo core are SRs, 31 ± 14 per cent. We find no increase of the slow rotator fraction in the core of the Coma cluster relative to the core of the Virgo cluster, despite a factor 24 increase in the local environmental density.

We note that the galaxies we identify as FRs are, on average, found at lower λ_R than those in the Virgo cluster from the ATLAS^{3D} survey (compare the blue crosses to the black datapoints in Figure 2). The mean λ_R for FRs in our sample is 0.21 ± 0.07; for the ATLAS^{3D} Virgo FRs over the range in ϵ covered by our sample the value is 0.33 ± 0.14. While our FRs in the Coma cluster are offset in λ_R, the two sets of FRs are consistent within the errors. In our sample we are missing high $\lambda_R (> 0.6)$ FRs frequently found in the ATLAS^{3D} sample. This is likely due to our sample missing very
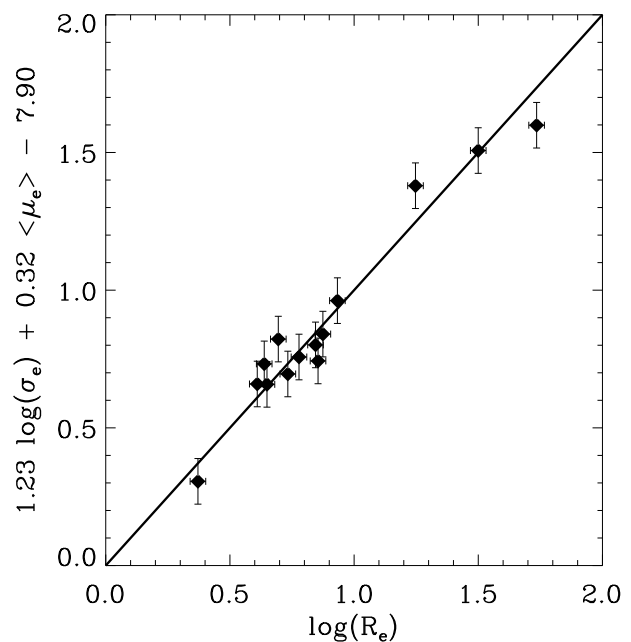
Figure 4. The FP determined from the SWIFT IFS Coma ETG sample determined by minimising the residuals orthogonal to the plane. The error on σ_e was determined by pPXF (typically 7.5 per cent) and the R$_e$ and $\langle \mu_e \rangle$ errors are based on the results of growth curve fits with different levels of sky subtraction. (typically 10 per cent in R$_e$ and $\langle \mu_e \rangle$).

flattened galaxies. This lack of flattened systems may be a property of the Coma cluster itself – the ϵ distribution of Coma ETGs in the Scodeggio et al. (1998) catalogue our sample is drawn from has more low ϵ galaxies than the ATLAS^{3D} sample – or it may be due to the unclear nature of the Scodeggio et al. (1998) sample selection. A larger IFS sample is required to determine if the FR population of the Coma cluster is consistent with that of the ATLAS^{3D} survey.

5 THE FUNDAMENTAL PLANE OF COMA EARLY-TYPE GALAXIES

We delay a detailed discussion of the FP for ETGs in the Coma cluster, using our enlarged final sample, to a future paper; here we simply present the best-fitting FP for our initial sample. We determine the FP by minimising the residuals orthogonal to the plane, as described in Jorgensen et al. (1996). This gives a FP of the form:

$$\log R_e = (1.23 \pm 0.13) \log \sigma_e + (0.32 \pm 0.03) \log \langle \mu \rangle_e - c$$

The errors are determined by a bootstrap procedure and the rms residuals in $\log R_e$ are 0.08. This projection of the data is shown in Figure 4. Jorgensen et al. (1996) determined the Coma FP from a sample of 79 ETGs with ground-based photometry and central σ_c (measured in a fixed physical aperture of 0.87 kpc) for each galaxy. Thomas et al. (2011) also determined the Coma FP from a sample of 16 ETGs but made use of composite HST and ground-based photometry and multiple long slit apertures for each galaxy. The FP coefficients we find are consistent with those studies (and others from the literature). However, our use of σ_e is an improvement over the traditional σ_c: Cappellari et al. (2006) show that, for a given σ_c, σ_e varies by up to 30 per cent. For similar sample sizes, our FP residuals are ~ 13 per cent smaller than those of Thomas et al. (2011), consistent with the ~ 15 per cent reduction in scatter found

by Falcón-Barroso et al. (2011) when moving from σ_c to σ_e. Detailed dynamical modelling of our IFS data would be desirable to recover dynamical masses and M/Ls and explore the mass fundamental plane (Thomas et al. 2011).

6   DISCUSSION

In Section 4 we presented tentative evidence that the fraction of SRs (relative to the number of FRs) is enhanced in the core of the Coma cluster, in comparison to both the less-massive Virgo cluster and the field population. This is consistent with the findings of Cappellari et al. (2011b), that the SR fraction increases only in the dense core of the Virgo cluster and not in the less dense outskirts of the cluster. This suggests that whatever mechanism forms SRs operates efficiently only in high density environments. Perhaps more significantly, we do not observe an increase in the SR fraction in the core of the Coma cluster relative to the core of the Virgo cluster, despite a factor 24 difference in the local density between the two environments. This suggests that whatever mechanism is responsible for the increase in the SR fraction does not depend in a simple way on the local environmental density.

To form a slow rotator it is likely that two ingredients are required: i) to remove (or cut off) the cold gas supply and ii) some form of dynamical interaction to remove the angular momentum of the galaxy. The hot intergalactic medium found in cluster environments can be effective both in ram-pressure stripping existing gas from a galaxy (Giovanelli & Haynes 1985; Morganti et al. 2006) and in preventing the acquisition of new gas by cold accretion (Oosterloo et al. 2010) or recycling of stellar mass loss (Leitner & Kravtsov 2011). While interactions are more common in dense environments these interactions tend to occur at high relative velocities, hence the dynamical effects are small (but see Tillson et al. 2011). Moore et al. (1999) suggest that dynamical pre-processing in in-falling groups enhances the historical number of low-velocity interactions for galaxies in massive clusters. This suggests a scenario where galaxies have their total angular momentum reduced through numerous major and/or minor mergers as they fall into a massive cluster, where the increased density of the hot IGM inhibits the regrowth of a high angular momentum component. It is unclear whether there is a critical threshold in the IGM density which prevents the reacquisition of angular momentum by a galaxy – we plan to obtain IFS observations of a larger sample of galaxies to be able to draw firm conclusions.

7   ACKNOWLEDGEMENTS

REFERENCES

Abazajian K. N. et al., 2009, ApJS, 182, 543
Berriman G. B. et al., 2004, in Proc. SPIE Vol. 5493, Optimizing Scientific Return for Astronomy through Information Technologies, P. J. Quinn & A. Bridger, ed., Vol. 5493, Bellingham, pp. 221–232
Binney J., 1982, AR&A, 20, 399
Binney J., Merrifield M., 1998, Galactic Astronomy. Princeton Univ. Press, Princeton, NJ
Bolton A. S., Burles S., Treu T., Koopmans L. V. E., Moustakas L. A., 2007, ApJL, 665, L105
Cappellari M., 2002, MNRAS, 333, 400
Cappellari M. et al., 2006, MNRAS, 366, 1126
Cappellari M., Copin Y., 2003, MNRAS, 342, 345
Cappellari M., Emsellem E., 2004, PASP, 116, 138
Cappellari M. et al., 2007, MNRAS, 379, 418
Cappellari M. et al., 2011a, MNRAS, 413, 813
Cappellari M. et al., 2011b, MNRAS, 416, 1680
Cenarro A. J., Cardiel N., Gorgas J., Peletier R. F., Vazdekis A., Prada F., 2001, MNRAS, 326, 959
Davies R. L., Efstathiou G., Fall S. M., Illingworth G., Schechter P. L., 1983, ApJ, 266, 41
de Zeeuw P. T. et al., 2002, MNRAS, 329, 513
Djorgovski S., Davis M., 1987, ApJ, 313, 59
Dressler A., 1980, ApJ, 236, 351
Dressler A., Lynden-Bell D., Burstein D., Davies R. L., Faber S. M., Terlevich R., Wegner G., 1987, ApJ, 313, 42
Emsellem E. et al., 2011, MNRAS, 414, 888
Emsellem E. et al., 2007, MNRAS, 379, 401
Falcón-Barroso J. et al., 2011, MNRAS, 417, 1787
Giovanelli R., Haynes M. P., 1985, ApJ, 292, 404
Hammer D. et al., 2010, ApJS, 191, 143
Hanuschik R. W., 2003, A&A, 407, 1157
Jorgensen I., Franx M., Kjaergaard P., 1996, MNRAS, 280, 167
Leitner S. N., Kravtsov A. V., 2011, ApJ, 734, 48
Moore B., Ghigna S., Governato F., Lake G., Quinn T., Stadel J., Tozzi P., 1999, ApJL, 524, L19
Morganti R. et al., 2006, MNRAS, 371, 157
Mould J. R. et al., 2000, ApJ, 529, 786
Oosterloo T. et al., 2010, MNRAS, 409, 500
Renzini A., Ciotti L., 1993, ApJL, 416, L49
Scodeggio M., Giovanelli R., Haynes M. P., 1998, AJ, 116, 2738
Sparke L. S., Gallagher, III J. S., 2007, Galaxies in the Universe - 2nd Edition. Cambridge Univ. Press, Cambridge
Thatte N., Tecza M., Clarke F., Goodsall T., Lynn J., Freeman D., Davies R. L., 2006, in Proc. SPIE Vol. 6269, Ground-based and Airborne Instrumentation for Astronomy, S. M. I., M. I., eds., Vol. 6269, Bellingham
Thomas J. et al., 2011, MNRAS, 415, 545
Tillson H., Miller L., Devriendt J., 2011, MNRAS, 417, 666
van Dokkum P. G., 2001, PASP, 113, 1420

York D. G. et al., 2000, AJ, 120, 1579